Altered precipitation dynamics lead to a shift in herbivore dynamical regime

Adam Pepi[1,2]*, Marcel Holyoak[3], Richard Karban[2]

[1]Graduate Group in Ecology, University of California Davis, Davis CA 95616

[2]Department of Entomology and Nematology, University of California Davis, Davis CA 95616

[3]Department of Environmental Science and Policy, University of California Davis, Davis CA 95616

*Corresponding author. Email: adampepi@gmail.com

Keywords: climate change, population dynamics, stochastic resonance, delayed density-dependence

Type of article: Letter

Abstract word count: 147

Main text word count: 3882

Number of references: 43

Number of figures: 4

Number of text boxes: 0

Number of tables: 1

***Statement of authorship*:** AP, RK, and MH conceived the study, AP conducted the analyses and wrote the manuscript, RK collected the census data, and RK and MH provided editorial advice.

***Data accessibility statement*:** The supporting data will be archived in HAL upon publication.

Abstract

The interaction between endogenous dynamics and exogenous environmental variation is central to population dynamics. Although investigations into the effects of changing mean climate is widespread, changing patterns of variation in environmental forcing also affect dynamics in complex ways. Using wavelet and time-series analyses, we identify a regime shift in the dynamics of a moth species in California from shorter to longer period oscillations over a 34-year census, and contemporaneous changes in regional precipitation dynamics. Simulations support the hypothesis that shifting precipitation dynamics drove changes in moth dynamics, possibly due to stochastic resonance with delayed density-dependence. The observed shift in climate dynamics and the interaction with endogenous dynamics mean that predicting future population dynamics will require information on both climatic shifts and their interaction with endogenous density dependence, a combination that is rarely available. Consequently, models based on historical data may be unable to predict future population dynamics.

Introduction

The dynamics of populations reflect the interplay between endogenous demographic and exogenous environmental drivers. Since its inception, population ecology has focused on debates about the relative contribution of these components to the generation of several salient phenomena observed in the dynamics of natural and laboratory populations, particularly cyclic fluctuations (Nicholson 1933; Andrewartha & Birch 1954; Barraquand *et al.* 2017). More recently, it has been recognized that both endogenous and exogenous drivers play important roles in generating observed population dynamics, and that endogenous deterministic dynamics and exogenous environmental noise or perturbations may combine to generate differing dynamics than would be expected for either component alone (Bjørnstad & Grenfell 2001; Turchin 2003; Barraquand *et al.* 2017). There has been additional motivation to understand the effects of climate on population dynamics as the effects of global climate change on the planet's biota have become more apparent (Walther *et al.* 2002; Parmesan 2006). Climate change is

expected to result in increased climate variability (Coumou & Rahmstorf 2012), as well as alterations to patterns of large-scale climate oscillations (Simon Wang *et al.* 2017), both of which are important drivers of local population dynamics. In a prominent example, changes in oceanic temperature oscillation regimes have resulted in dramatic changes to precipitation patterns in California (Simon Wang *et al.* 2017), with large impacts to society and natural ecosystems.

Climate variation can have direct effects on interannual fluctuations in population size or may interact in complex ways with endogenous dynamics of populations. For example, environmental perturbations can sustain population oscillations that might otherwise decay to a stable equilibrium (Tomé & De Oliveira 2009; Barraquand *et al.* 2017). Climate change has also appeared to cause the collapse of population cycles of many species across Europe (Ims *et al.* 2008; Cornulier *et al.* 2013). Environmental perturbations with different spectra of variability can also amplify, dampen, or impose their own spectra on oscillatory populations depending on the "colour" (temporal autocorrelation) of environmental spectra relative to the spectra of the endogenous dynamics of the population (Greenman & Benton 2003). Changing climate can also interact in a non-stationary way with population dynamics, such as transient effects of long-term climate oscillations on epidemic disease cycles (Rodó *et al.* 2002; Cazelles *et al.* 2005). However, testing for such effects on population dynamics of other kinds of organisms requires rarely available long-term population data.

In the present study, we examined how changing precipitation dynamics interact with the endogenous population dynamics of an extensively studied insect species, the Ranchman's tiger moth (*Arctia virginalis*). We analyzed 34 years of census data from northern California, over a period during which there have been significant shifts in the dynamics of regional climate (Simon Wang *et al.* 2017). Using time series analyses and simulations, we tested for changes in population dynamics, and compared multiple possible mechanisms for observed shifts. Using simulations, we tested the hypotheses that shifting dynamics were because 1. underlying dynamics were first masked and later amplified by precipitation, 2. underlying dynamics were first amplified and later masked by

precipitation, or 3. dynamical shifts were driven completely exogenously by changing precipitation dynamics.

Materials & Methods

Description of system

Ranchman's tiger moth (*Arctia virginalis*) is a univoltine, day-active Arctiine moth, native to much of the western United States. Adult moths emerge in late spring or early summer and have a flight period of several weeks during which they do not feed. Eggs are laid on low vegetation or litter in early summer; small caterpillars hatch soon after eggs are laid. Early instar caterpillars are heavily preyed upon by ground nesting ants, and are potentially food-limited during seasonal senescence of vegetation in Mediterranean summers (Karban *et al.* 2013, 2017). Time series analyses have shown that greater precipitation during the previous year results in greater population growth, possibly due to increased food availability during the summer drought (Karban & de Valpine 2010; Karban *et al.* 2017). Caterpillars feed continuously over the winter period and do not diapause in California. After this, they move up to feed on higher vegetation and become more visible in late winter in California. Caterpillars are generalists, with a preference for alkaloid-containing hosts (English-Loeb *et al.* 1993; Karban *et al.* 2010). Caterpillars are also frequently attacked by tachinid parasitoids, *Thelaira americana* (Karban & de Valpine 2010), which are specialists on Arctiine moths (Arnaud 1978), and may functionally be specialists on Ranchman's tiger moth at our study site, the Bodega Marine Reserve. However, analyses have suggested that parasitism has little effect on caterpillar population dynamics (Karban & de Valpine 2010). Caterpillar populations at the Bodega Marine Reserve and other sites often exhibit high mortality rates after high population density years due to a granulovirus. Monitoring at Bodega and other sites has shown delayed density-dependent infection and mortality rates due to granulovirus (Pepi, Pan & Karban, unpublished data).

Censuses

Caterpillar censuses were conducted on perennial evergreen yellow bush lupine (*Lupinus arboreus*) bushes at Bodega Marine Reserve in Sonoma County, California (38°19'05"N, 123°04'12"W). The number of caterpillars on 10 lupine bushes in the same patch were counted yearly from 1986 to 2019 (>10 in 1986). Bushes were censused in the last week of March each year. Previous repeated censuses within a year between late February and the end of March suggest that population estimates were unlikely to vary significantly due to changes in seasonal phenology from year to year (Karban and Grof-Tisza, unpublished data), because of the long development period of caterpillars and their limited mobility during this stage. The same lupine bushes were censused each year; however, the identity of bushes changed because these lupines were short lived (< 7yr). To account for variation in sampling effort, area of each lupine bush censused was measured to calculate caterpillar density per m^2 (plotted as caterpillars per 100 m^2 in Figure 3 for legibility). Precipitation was recorded at the site as part of ongoing climate monitoring by the University of California and using a rain gauge at the study site (US Weather Bureau type manual rain gauge prior to 1992 and an optical rain gauge ORG-815, Optical Scientific, Gaithersburg, MD since 1992 with a Hydrological Services TB4 tipping bucket, Campbell Scientific, Ogden, UT since 2003). For analyses, total annual precipitation within the hydrologic year was calculated (from October 1st of the previous year to September 30th of the current year).

Statistical analyses

To test for non-stationary relationships between precipitation and caterpillar dynamics over time, wavelet analysis was conducted separately on logged and scaled caterpillar and scaled precipitation time series, and as wavelet coherence analyses on both series (Figure 3). Scaling was accomplished by subtracting the mean and dividing by the standard deviation (scale() in R). Analyses were conducted using the package BIWAVELET (Gouhier *et al.* 2019), using Morlet wavelet transforms. In addition, change-point analyses were conducted using the SEGLM and TSDYN packages (Antonio & Stigler 2009; Stigler 2019), with a model containing direct and delayed density-dependence, and a

125 separate model also including precipitation as a covariate. We included precipitation as a covariate
126 based on previous knowledge that precipitation was important to dynamics. We included direct density-
127 dependence based on previous detection in time series analyses (Karban & de Valpine 2010), and
128 delayed density-dependence based on wavelet periodogram results and the observation of delayed-
129 density dependent mortality from granulovirus in field studies (Pepi, Pan & Karban, unpublished data).
130 Models with and without a threshold (C) were compared using AIC. Break point models were of the
131 form:

132 $$X_t \sim Normal(\ a_{0,1} + a_{1,1}X_{t-1} + a_{2,1}X_{t-2} + \beta_{1,1}Precip_{t-1}, \sigma_1^2) \ \mid \ t \leq C$$

133 $$X_t \sim Normal\left(a_{0,2} + a_{1,2}X_{t-1} + a_{2,2}X_{t-2} + \beta_{1,2}Precip_{t-1}, \sigma_2^2\right) \mid \ t \geq C,$$

134 in which X_t is log population density [$ln(count/area)$], a_0 is the intercept, a_1 is direct density
135 dependence, a_2 is delayed density dependence, and β_1 is the effect of precipitation, σ^2 is the variance,
136 with a separate parameter estimate for each before and after the threshold.

137 Bayesian state space population models using a Poisson observation process were constructed
138 to test for direct and delayed density-dependence and effects of precipitation. We conducted this as a
139 separate step from testing for thresholds to avoid identifiability issues due to limited data availability.
140 We primarily examined a model with the same process structure as breakpoint models, including direct
141 and delayed density dependence and an effect of precipitation, based on *a priori* knowledge about the
142 system. For comparison, models with all possible combinations of variables were generated and
143 compared using WAIC (Vehtari et al. 2017). State space models were fit to the time series from 1986-
144 2004 and 2004-2019 separately and results compared, based on findings of change-point analyses. The
145 full state-space model was of the form:

146 $$Y_t \sim Poisson(\exp(X_t) * area_t)$$

147 $$X_t \sim Normal(a_0 + a_1X_{t-1} + a_2X_{t-2} + \beta_1 Precip_{t-1}, \sigma^2\ ),$$

in which Y_t is caterpillar count, X_t is the estimated population density state on a log scale, $area_t$ is the area of lupine sampled, a_0 is the intercept, a_1 is direct density dependence, a_2 is delayed density dependence, β_1 is the effect of precipitation, and σ^2 is the process variance. Models were fitted in JAGS with interface in R using RJAGS (Plummer 2019) and R2JAGS (Yu-Sung Su & Yajima 2015). We used a vague regularizing Gaussian prior for all parameters [$Normal(0, 10)$], except for the process variance (σ^2), for which we used a uniform prior [$Uniform(0, 10)$]. Model convergence was assessed using the CODA (Martyn *et al.* 2019) package, by visualizing chains (Figures S1-3) and the $\hat{R}$ convergence criterion (Gelman & Rubin 1992). We also conducted one-step ahead simulations as posterior predictive checks (Figures S4-6), for which P-values were 0.5±0.03, indicating acceptable model fit. Models were fitted using 3 MCMC chains of 20,000 iterations, with 1,000 iterations of burn-in. All $\hat{R}$ values were <1.001.

To ascertain the mechanisms driving shifts in dynamics, we conducted deterministic simulations by projecting populations into the future using parameter values sampled from the posteriors of fitted state space process models. Simulations were also conducted with fitted density-dependence parameters, but with all precipitation effects drawn from the posterior of the model with the highest estimated effect of precipitation (from the second half of the series; β_1=0.922). Another simulation was conducted using the fitted process model from the second part of the series, but with density-dependent parameters (a_1, a_2) set to zero. For simulations, observed starting population sizes were used, and observed precipitation values were used for the entire period. For each mechanistic scenario, 10,000 simulations were conducted, each based on a separate draw from posteriors. Simulated population trajectories were wavelet transformed, and a dissimilarity relative to the true population series was calculated based on the method of Rouyer *et al.* (2008b) (Table S3, Figures S7-8), all using BIWAVELET (Gouhier *et al.* 2019).

Results

Caterpillar population dynamics exhibited a clear regime shift during our study. Wavelet spectrograms show that dominant oscillatory periods of caterpillar and precipitation dynamics shifted from short-period (2-3 yr) to long-period oscillations (4-6 yr; Figure 1c,e), though periodicity was only significant at the 95% level for precipitation in the first part of the series (2-3 yr periodicity from ~1992-1999) and caterpillars in the second part of the series (4-6 yr periodicity from ~2003-2013). Precipitation dynamics changed after ca. 1999, and caterpillar dynamics changed shortly thereafter (ca. 2002). Wavelet coherence between precipitation and caterpillar numbers shifted from a 3-year period in the early part of the series to a 3-6 year period after ca. 2005 (Figure 1g), suggesting a role of precipitation in shifts in caterpillar population dynamics. The observed shift in precipitation dynamics in turn was likely caused by shifting oceanic climate oscillations; the Pacific Decadal Oscillation and offshore sea surface temperature switched from a warm to a cold phase after 1999, which resulted in shifts in dynamics of several marine species at that time (Cloern *et al.* 2010; Thomson *et al.* 2010). A similar climate regime of high-amplitude, long-period oscillations between multi-year drought and high precipitation is expected to be the norm for California in the future (Swain *et al.* 2018).

Change-point analyses found a change in dynamics with a threshold in 2002 (ΔAIC=4.8 relative to model without a threshold) in a model without precipitation, or in 2004 in a model including precipitation (ΔAIC=6.5). Before the threshold, direct density-dependence was estimated to be negative and this became positive after the threshold, though there was limited evidence that these estimates were different from zero ($0.10>P>0.09$; see Table 1). In models that included precipitation, its effects were always near zero before the threshold, and strongly positive after the threshold (Table 1). Delayed density-dependence had negative parameter estimates in all models, with the most evidence for delayed density dependence after the threshold in the model without precipitation ($P=0.019$), and weaker evidence otherwise ($P>0.2$).

Results from Bayesian Poisson state-space models corresponded broadly with those from the change point analyses, showing a shift in dynamics from the first to the second period. The full model

was an acceptable fit relative to other model structures tested, though large differences were not detected due to the state-space structure and limited data availability (Table S1; ΔWAIC<2 for all models). 90% high density posterior intervals (HDPI) that are superior for characterizing MCMC posteriors (because of more samples in the tails; Kruschke 2014) show the following: Considering the full model fitted to the entire series (1986-2019), direct density-dependence was weak (a_1 =-0.11; 90% HDPI: -0.23 – 0.47), delayed density-dependence was negative (a_2 =-0.3 ; 90% HDPI: -0.63 – 0.03]), and there was a weak positive effect of rainfall (β_1 =0.30; 90% HDPI: -0.08 – 0.70; Figure 2). For the first part of the series (1986-2004), direct density-dependence was negative (a_1 =-0.63; 90% HDPI: -1.19 – -0.10), delayed density-dependence was negative but weak (a_2 =-0.27; 90% HDPI: -0.78 – 0.26), and the effect of precipitation was weak (β_1 =0.26; 90% HDPI: -0.17 – 0.68; Figure 2). For the second part of the series (2004-2019), direct density-dependence was positive (a_1 =0.46; 90% HDPI: 0.03 – 0.82), delayed density-dependence was negative but weak (a_2 =-0.19; 90% HDPI: -0.63 – 0.36), and the effect of precipitation was stronger and positive (β_1 =0.92; 90% HDPI: 0.2 – 1.75; Figure 2). Overall, the results of these models provide evidence for a shift from negative to positive direct density-dependence from the first to the second part of the series, with non-overlapping 90% intervals between the two parts (a_1 =-1.19 – -0.13 vs. 0.03 – 0.82), although 95% intervals did have a marginal overlap (a_1 =-1.29 – 0.03 vs. -0.05 – 0.96; Figure 2). This corresponds with a shift from type III to type IV dynamics (Figure 3) and a shift from shorter to longer period dynamics.

The results from simulation analyses suggested that the long-period dynamics observed in the second part of the series (2004-2019) could best recreate the observed dynamics. Specifically, there was some evidence that endogenous dynamics as parameterized from the second part of the series best recovered the observed shift in dynamical regime when used to simulate dynamics for the entire series, based on the maximum *a posteriori* dissimilarity calculated from wavelet transforms (Figure 4, S1,Table S3; Rouyer *et al.* 2008; Gouhier *et al.* 2019). This was the case both in simulations which

used the original fitted precipitation parameters, and in simulations in which the effect of precipitation was set to the same value to examine solely the effect of different endogenous dynamics (lowest dissimilarity: d=17.6; whole series: d=22.1, 18.5; first part: d=22.8, 21.4; Figure 4, S1, Table S3). Simulations including density-dependence reproduced dynamics somewhat better (d=17.6) than simulations without density-dependence (d=19.7). The broad posterior intervals of simulation results indicated substantial uncertainty as to the mechanisms driving observed shifts (Figure 4). However, to the extent that we are interested in the question of whether specific endogenous dynamics (i.e., specific parameter values) underlie the observed shift in dynamics, the point estimates from the second part of the series best reproduced dynamics. Overall, results were consistent with the interpretation that the shift in dynamics was driven either by an interaction between endogenous dynamics and precipitation, or possibly solely by precipitation (Figure 4).

Discussion

Our analyses together suggest that over the census period, the changing structure of variation in precipitation dynamics interacted with the structure of endogenous dynamics of caterpillar populations to generate novel dynamics. This resulted in higher amplitude, long-period oscillations in the second part of the series (2004-2019), in which both the lowest (2005) and the highest (2019) caterpillar population densities were observed. This is in contrast with the first part of the census (1986-2004) which was characterized by weak lower amplitude and short-period oscillations. These shifts in oscillatory period corresponded with a shift from negative direct and delayed density-dependence (type III dynamics) to positive direct and negative delayed density dependence (type IV dynamics). Although many parameter posterior intervals overlapped zero, there was strong statistical evidence for our main hypothesis, showing a shift from direct density-dependence to negative density dependence during the study (Figure 2,3). This shift in dynamics appears to have been due to changing patterns of variation in environmental forcing and illustrates the complexity of forecasting impacts of changes in both mean and pattern of variation in future climates on population dynamics.

Simulation studies have shown that environmental noise can resonate with the dominant period of deterministic endogenous dynamics of a system if the noise spectra includes the period of the deterministic system (Royama 1992; Alonso *et al.* 2007). Environmental variation may also impose its own spectral signature on population dynamics with different dominant periods (Greenman & Benton 2003). Given these observations, there are multiple possible mechanistic explanations for the shift in dynamics observed in this study. One possible interpretation is that the interaction between the endogenous dynamical structure of this population with changing exogenous perturbation (i.e., precipitation) obscured the endogenous dynamics in one part of the series, but not the other (Ranta *et al.* 2000). Another interpretation is that dynamical shifts may have been entirely externally forced by changing precipitation dynamics. We distinguished between these possibilities by simulating deterministic population trajectories from fitted state-space models using observed precipitation, which indicated that the dynamics from the second part of the series were somewhat more likely to have represented the underlying endogenous dynamics of the system. This indicates that short-period oscillations in precipitation may have interfered with delayed density-dependence in the endogenous dynamics to generate the observed population dynamics in the first half of the caterpillar time series. By imposing short-period oscillations onto population dynamics, external forcing by precipitation may have created only the appearance of negative direct density-dependence. During the second half of the series, longer period oscillations of precipitation may have resonated with delayed density-dependence and generated high-amplitude long-period oscillations. This interpretation is supported by the fact that simulations including negative direct density-dependence (*i.e.*, the model from the first part of the series) prevented the resonance of precipitation with delayed density-dependence and did not recreate the original dynamics quite as effectively as models with positive direct density-dependence (Figure 4, S7-8, Table S3). Furthermore, the possibility that observed shifts in dynamics were driven completely externally by precipitation seems less likely because simulations lacking density-dependence did not as effectively recover the original shift in dynamics as simulations including density-dependence.

However, if we consider the uncertainty of parameter estimates in the simulation results, we cannot be confident in distinguishing between alternative scenarios, as all simulation posteriors overlap substantially (Figure 4). Nonetheless, despite the limited information contained within our 34-year population time series, our simulations allowed us to compare the relative evidence for alternate mechanisms that might have caused the observed shift.

The dynamics that we describe during the first part of the series are consistent with previous work, which indicated that precipitation positively affects caterpillar population growth rates and interacts with endogenous dynamics of overcompensating negative direct density-dependence (Karban & de Valpine 2010; Karban *et al.* 2017). Mechanisms proposed to explain the effect of precipitation include limited resources during summer drought (Karban & de Valpine 2010), or negative effects of precipitation on predatory ants (Karban *et al.* 2017). Parasitism and viral infection are potential mechanisms for both direct and delayed density-dependence in this population, as they are in many insects and particularly Lepidoptera (Myers & Cory 2013, 2016). Parasitism and viral infection can induce density-dependence in insect population dynamics when parasitoids are host-specific and display numerical responses to host density, and when virus transmission depends on host density (Myers & Cory 2013). Delays in the action of density-dependence may be caused by delayed numerical responses of parasitoids (Myers & Cory 2013), or a greater prevalence of covert viral infections or viral occlusion bodies in the environment after high-density years (Myers & Cory 2016). Long-term monitoring data revealed no delayed density-dependent parasitism in this population (Karban & de Valpine 2010). However, laboratory rearing of *A. virginalis* from multiple monitored populations suggested a delayed-density dependent rate of viral infection (Pepi, Pan & Karban, unpublished data) as is the case in many Lepidoptera (Anderson & May 1980; Myers & Cory 2013, 2016).

In contrast, the dynamics of the second part of the series (2004-2019) were not predictable from our previous understanding of caterpillar population dynamics derived from analyses of time series that were long by ecological standards (20 years, 1986-2006; Karban & de Valpine 2010). This type of

non-stationarity due to shifts in climatic regimes has large implications for forecasting and managing populations of threatened or pest species, because such shifts have the potential to obfuscate predictions about management actions. Ecological forecasting has become an urgent goal in light of global change and unprecedented human pressures on the biosphere (Clark *et al.* 2001). Whereas most literature has focused on predicting ecological state variables (e.g., population size; Dietze 2017) , we examined how changing patterns of climate interacted with endogenous population drivers to qualitatively change dynamics. This illustrates the importance of considering the interaction between endogenous population drivers and exogenous climate variation in projecting population dynamics into the future, and argues that incorporating changes in patterns of climate into predictions is essential.

The fact that the qualitative range of dynamics in populations is to some extent limited (i.e., there are not ten million types of population dynamics; Lawton 1992) makes predicting shifts in population dynamics due to climate change a more attainable prospect. Consistent with this, most populations have either first or second order, and either chaotic or non-chaotic dynamics (Types I-IV and I'-IV' in Fig. 2; also see Royama 1992), in addition to some other important axes of variation (Turchin 2003; Barraquand *et al.* 2017). Ecologically, the presence of overcompensating (type II-III) density dependence, a stable equilibrium (type I), or longer period cycles (type IV) have important effects on species interactions, ecosystem dynamics, and how climate is likely to affect dynamics (Ranta *et al.* 2000; Ims *et al.* 2008). Mechanistic studies separating endogenous from exogenous components of dynamics can distinguish whether observed dynamics, such as cycles, arise from different mechanisms. Some of these mechanisms include self-sustaining or noise-sustained second order dynamics, externally-forced first order dynamics (Barraquand *et al.* 2017), and non-cyclic dynamics that mask endogenous second-order dynamics, as we found support for in the present study (Greenman & Benton 2003). The application of methods such as those implemented in the present study can help distinguish between different possible combinations of endogenous and exogenous components of a system that might have generated the observed dynamics. Doing so will improve our

ability to understand how changes in exogenous forcing due to climate change are likely to affect future population dynamics.

Acknowledgments

Many former students of RK contributed to census data collection, and this work would not have been possible without them. These censuses were conducted at the UC Bodega Marine Reserve and we thank Peter Connors and Jackie Sones for facilitating our work there. We would also like to thank Eric Post, Jay Rosenheim, Rolf Ims, and Louis Botsford for help improving the manuscript. This work has been supported by NSF, most recently NSF-LTREB-1456225

Data Accessibility

Data will be archived on HAL upon acceptance.

References

Alonso, D., McKane, A.J. & Pascual, M. (2007). Stochastic amplification in epidemics. *J. R. Soc. Interface*, 4, 575–582.

Anderson, R.M. & May, R.M. (1980). Infectious Diseases and Population Cycles of Forest Insects. *Science (80-.).*, 210, 658–661.

Andrewartha, H.G. & Birch, L.C. (1954). *The distribution and abundance of animals*. University of Chicago Press.

Antonio, F.D.N. & Stigler, J.L.A.M. (2009). tsDyn: Time series analysis based on dynamical systems theory.

Arnaud, P.H. (1978). *Host Parasite Catalog of North American Tachinidae (Diptera)*. Department of Agriculture, Science and Education Administration.

Barraquand, F., Louca, S., Abbott, K.C., Cobbold, C.A., Cordoleani, F., DeAngelis, D.L., *et al.* (2017). Moving forward in circles: challenges and opportunities in modelling population cycles. *Ecol. Lett.*, 20, 1074–1092.

Bjørnstad, O.N. & Grenfell, B.T. (2001). Noisy clockwork: time series analysis of population

fluctuations in animals. *Science*, 293, 638–43.

Cazelles, B., Chavez, M., McMichael, A.J. & Hales, S. (2005). Nonstationary influence of El Niño on the synchronous dengue epidemics in Thailand. *PLoS Med.*, 2, 0313–0318.

Clark, J.S., Carpenter, S.R., Barber, M., Collins, S., Dobson, A., Foley, J.A., *et al.* (2001). Ecological forecasts: an emerging imperative. *Science (80-.).*, 293, 657–660.

Cloern, J.E., Hieb, K.A., Jacobson, T., Sans, B., Di Lorenzo, E., Stacey, M.T., *et al.* (2010). Biological communities in San Francisco Bay track large-scale climate forcing over the North Pacific. *Geophys. Res. Lett.*, 37, 1–6.

Cornulier, T., Yoccoz, N.G., Bretagnolle, V., Brommer, J.E., Butet, A., Ecke, F., *et al.* (2013). Europe-wide dampening of population cycles in keystone herbivores. *Science (80-.).*, 340, 63–66.

Coumou, D. & Rahmstorf, S. (2012). A decade of weather extremes. *Nat. Clim. Chang.*, 2, 491–496.

Dietze, M.C. (2017). Prediction in ecology: a first-principles framework. *Ecol. Appl.*, 27, 2048–2060.

English-Loeb, G.M., Brody, A.K. & Karban, R. (1993). Host-plant-mediated interactions between a generalist folivore and its tachinid parasitoid. *J. Anim. Ecol.*, 62, 465.

Gelman, A. & Rubin, D.B. (1992). Inference from iterative simulation using multiple sequences. *Stat. Sci.*, 7, 457–472.

Gouhier, T.C., Grinsted, A. & Simko, V. (2019). R package biwavelet: Conduct Univariate and Bivariate Wavelet Analyses.

Greenman, J. V. & Benton, T.G. (2003). The amplification of environmental noise in population models: Causes and consequences. *Am. Nat.*, 161, 225–239.

Ims, R.A., Henden, J.A. & Killengreen, S.T. (2008). Collapsing population cycles. *Trends Ecol. Evol.*, 23, 79–86.

Karban, R., Grof-Tisza, P. & Holyoak, M. (2017). Wet years have more caterpillars: Interacting roles of plant litter and predation by ants. *Ecology*.

Karban, R., Karban, C., Huntzinger, M., Pearse, I. & Crutsinger, G. (2010). Diet mixing enhances the

performance of a generalist caterpillar, Platyprepia virginalis. *Ecol. Entomol.*, 35, 92–99.

Karban, R., Mata, T.M., Grof-Tisza, P., Crutsinger, G. & Holyoak, M.A. (2013). Non-trophic effects of litter reduce ant predation and determine caterpillar survival and distribution. *Oikos*, 122, 1362–1370.

Karban, R. & de Valpine, P. (2010). Population dynamics of an Arctiid caterpillar-tachinid parasitoid system using state-space models. *J. Anim. Ecol.*, 79, 650–661.

Kruschke, J. (2014). Doing Bayesian data analysis: A tutorial with R, JAGS, and Stan.

Lawton, J.H. (1992). There are not 10 million kinds of population dynamics. *Oikos*, 63, 337–338.

Martyn, A., Best, N., Cowles, K., Vines, K., Bates, D., Almond, R., *et al.* (2019). Package ‘ coda ’: Output Analysis and Diagnostics for MCMC.

Myers, J.H. & Cory, J.S. (2013). Population Cycles in Forest Lepidoptera Revisited. *Annu. Rev. Ecol. Evol. Syst.*, 44, 565–592.

Myers, J.H. & Cory, J.S. (2016). Ecology and evolution of pathogens in natural populations of Lepidoptera. *Evol. Appl.*, 9, 231–247.

Nicholson, A.J. (1933). The balance of animal populations. *J. Anim. Ecol.*, 2, 132 – 178.

Parmesan, C. (2006). Ecological and evolutionary responses to recent climate change. *Annu. Rev. Ecol. Evol. Syst.*, 37, 637–669.

Plummer, M. (2019). rjags: Bayesian Graphical Models using MCMC.

Ranta, E., Lundberg, P., Kaitala, V. & Laakso, J. (2000). Visibility of the environmental noise modulating population dynamics. *Proc. R. Soc. B Biol. Sci.*, 267, 1851–1856.

Rodó, X., Pascual, M., Fuchs, G. & Faruque, A.S.G. (2002). ENSO and cholera: A nonstationary link related to climate change? *Proc. Natl. Acad. Sci. U. S. A.*, 99, 12901–12906.

Rouyer, T., Fromentin, J.-M., Stenseth, N.C. & Cazelles, B. (2008). Analysing multiple time series and extending significance testing in wavelet analysis. *Mar. Ecol. Prog. Ser.*, 359, 11–23.

Royama, T. (1992). *Analytical Population Dynamics*. Chapman & Hall, London.

Simon Wang, S.Y., Yoon, J.H., Becker, E. & Gillies, R. (2017). California from drought to deluge. *Nat. Clim. Chang.*, 7, 465–468.

Stigler, M. (2019). seglm: Segmented/threshold regression methods.

Swain, D.L., Langenbrunner, B., Neelin, J.D. & Hall, A. (2018). Increasing precipitation volatility in twenty-first-century California. *Nat. Clim. Chang.*, 8, 427–433.

Thomson, J.R., Kimmerer, W.J., Brown, L.R., Newman, K.B., Mac Nally, R., Bennett, W.A., *et al.* (2010). Bayesian change point analysis of abundance trends for pelagic fishes in the upper San Francisco Estuary. *Ecol. Appl.*, 20, 1431–1448.

Tomé, T. & De Oliveira, M.J. (2009). Role of noise in population dynamics cycles. *Phys. Rev. E - Stat. Nonlinear, Soft Matter Phys.*, 79, 1–8.

Turchin, P. (2003). *Complex Population Dynamics: A Theoretical/Empirical Synthesis*. Princeton University Press, Princeton.

Vehtari, A., Gelman, A. & Gabry, J. (2017). Practical Bayesian model evaluation using leave-one-out cross-validation and WAIC. *Stat. Comput.*, 27, 1413–1432.

Walther, G., Post, E., Convey, P., Menzel, A., Parmesan, C., Beebee, T.J.C., *et al.* (2002). Ecological responses to recent climate change. *Nature*, 416, 389–395.

Yu-Sung Su & Yajima, M. (2015). R2jags: Using R to Run “JAGS.”

Tables and Figures

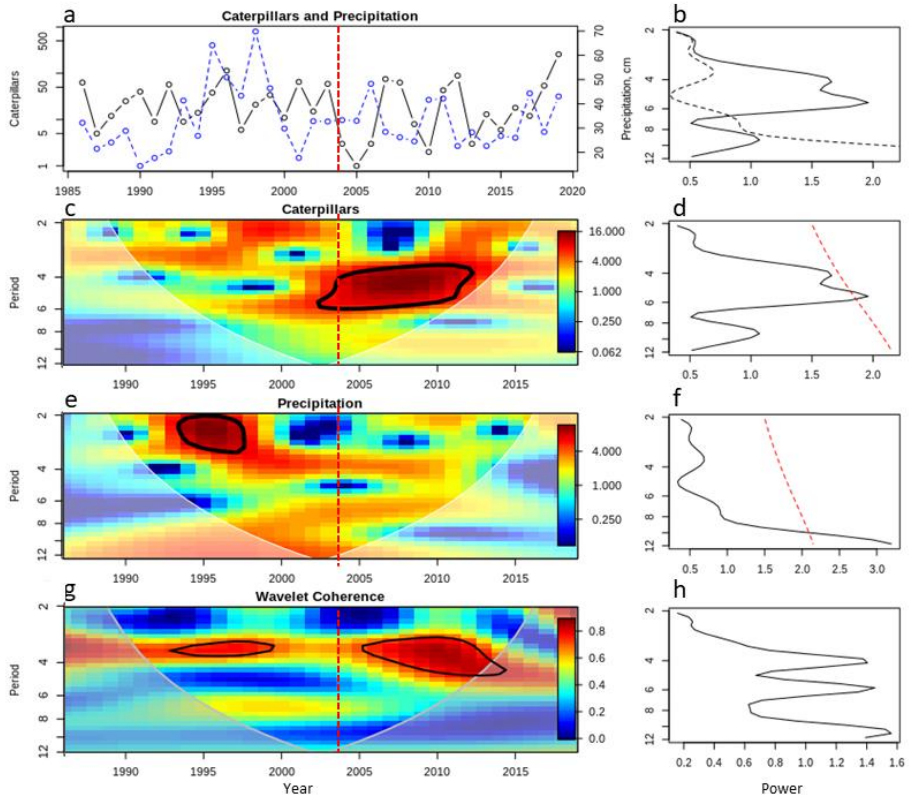

Figure 1: (a) Time series of caterpillar population counts per 100 m^2 (solid black line) and total annual precipitation (dashed blue line); (c) local wavelet transform of caterpillar population counts; (e) local wavelet transform of total annual precipitation; (g) wavelet coherence between total annual precipitation and caterpillar population counts; (b,d,f) global spectra of (a,c,e); (h) global coherence of (g), total annual precipitation and caterpillar population counts. The dashed red line through (a,c,e,g) represents the time threshold found in the change-point analysis including precipitation. Caterpillar density and spectral period are shown on a log scale; total annual precipitation is shown on the right axis. Solid black lines in (c,e,g) delimit regions of significant periodicity or coherence at a 95% confidence level from a bootstrap test. Color bars in (c,e,g) show the scale power from low (blue) to high (red). Caterpillar wavelet spectrum is shown in (a) with a solid line, and precipitation wavelet spectrum is shown with a dashed line. Dashed red lines in (d,f) show the 95% confidence threshold from a bootstrap test; peaks to the right of the line represent significant periodicity.

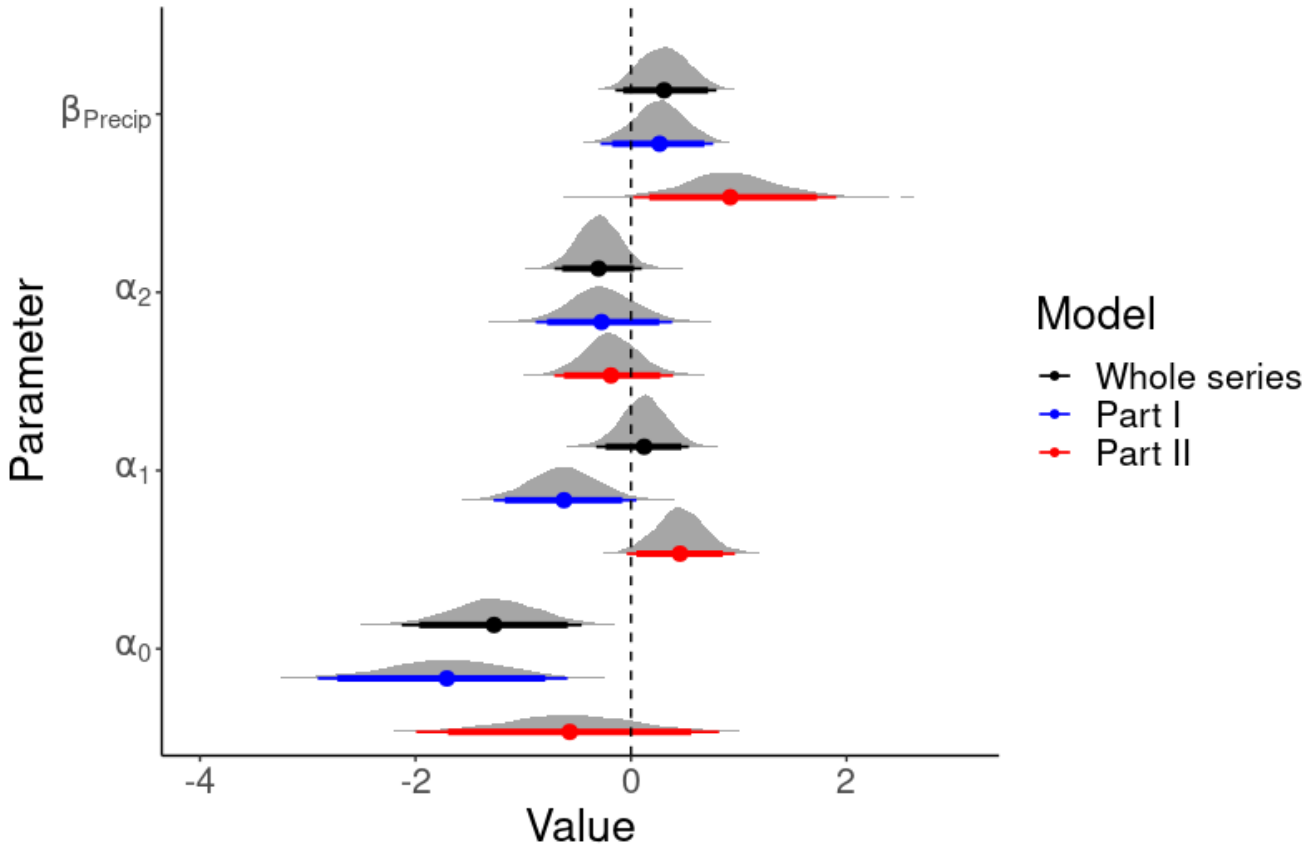

Figure 2: Bayesian posterior 90% and 95% (broad to narrow lines) posterior intervals, and point estimates of parameters from Poisson state-space models. Estimates from the whole series are shown in black (1986-2019), before the threshold in blue (1986-2004), and after the threshold in red (2004-2019).

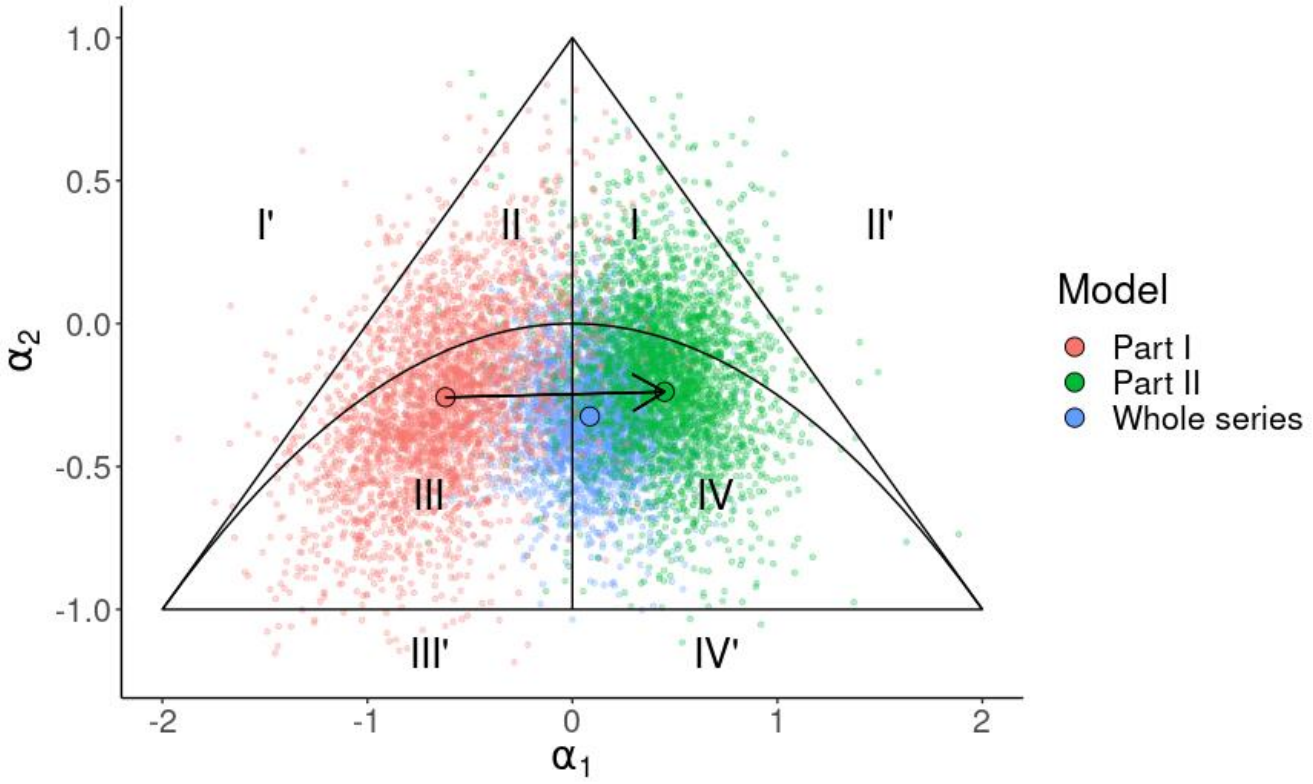

Figure 3. Posterior distributions of Bayesian state space models fit to the first part of the series (1986-2004), the second part of the series (2004-2019) and the whole series (1986-2019), plotted in the Royama parameter plane, showing a shift from type III to type IV dynamics. Open circles represent the median of the posterior distributions.

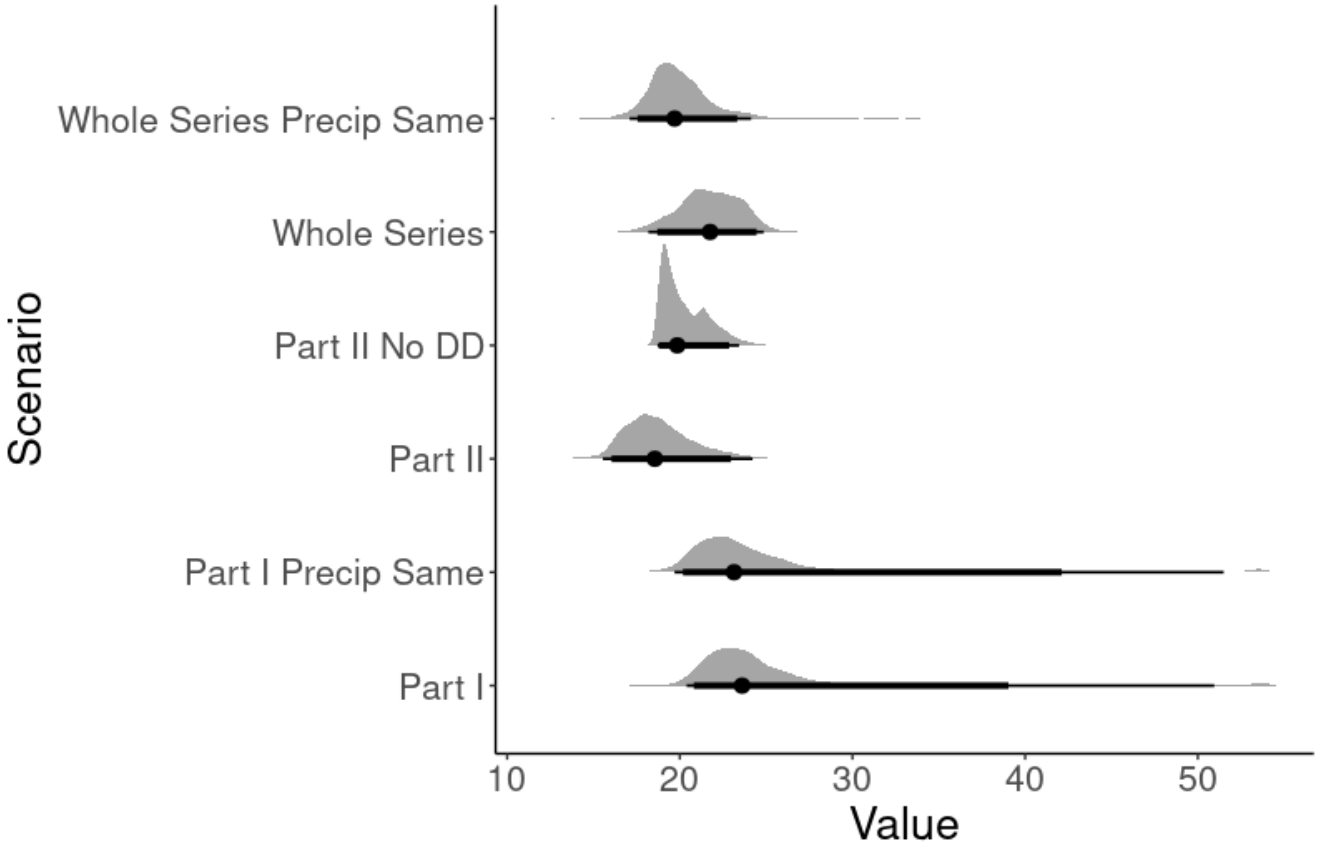

Figure 4. Simulation 90% and 95% (broad to narrow lines) posterior intervals and point estimates of dissimilarity values relative to the true population trajectories, from multiple mechanistic scenarios.

457

Model	Period	$a_{1\,[P]}$	$a_{2\,[P]}$	$\beta_{1[P]}$
Without Precipitation	**1986-2002**	-0.56 [P=0.098]	-0.44 [P=0.211]	
	2002-2019	0.35 [P=0.109]	-0.52 [P=0.019]	
With Precipitation	**1986-2004**	-0.57 [P=0.091]	-0.41 [P=0.209]	-0.01 [P=0.098]
	2004-2019	0.510 [P=0.027]	-0.286 [P=0.218]	1.27 [P=0.026]

458 **Table 1**. Results of change-point analysis, including parameter estimates and P values, from models
459 with and without precipitation, before and after change-point thresholds.

460

461

462

463

464

465

466

467

468

469

470

471

472

473

474

475

476

Supplementary Materials:

Process model	ΔWAIC	WAIC	a_0 [2.5%,97.5%]	a_1 [2.5%,97.5%]	a_2 [2.5%,97.5%]	β_1 [2.5%,97.5%]
1986-2019:						
$X_t \sim a_0 + a_1 X_{t-1} + a_2 X_{t-2} + \beta_1 Precip_{t-1}$	1.38	201.78	-1.28 [-2.13, -0.46]	0.11 [-0.31, 0.53]	-0.30 [-0.70, 0.01]	0.30 [-0.18, 0.78]
$X_t \sim a_0 + a_1 X_{t-1} + \beta_1 Precip_{t-1}$	1.00	201.40	-1.01 [-1.50, -0.52]	0.03 [-0.29, 0.35]	-	0.36 [0.01, 0.70]
$X_t \sim a_0 + a_1 X_{t-1} + a_2 X_{t-2}$	1.36	201.76	-1.34 [-1.62, -0.52]	0.11 [-0.32, 0.53]	-0.35 [-0.750, 0.05]	-
$X_t \sim a_0 + a_1 X_{t-1}$	0.96	200.76	-1.05 [-1.75, -0.36]	0.05 [-0.37, 0.46]	-	-
$X_t \sim a_0 + \beta_1 Precip_{t-1}$	**0.0***	**200.4***	0.05 [-0.28, 0.38]	-	-	0.40 [0.018, 1.04]
$X_t \sim a_0$	0.13	200.53	0.04 [-0.59, 0.68]	-	-	-
1986-2004:						
$X_t \sim a_0 + a_1 X_{t-1} + a_2 X_{t-2} + \beta_1 Precip_{t-1}$	0.52	117.37	-1.74 [-2.92, -0.61]	-0.63 [-1.29, 0.03]	-0.27 [-0.89, 0.34]	0.26 [-0.27, 0.78]
$X_t \sim a_0 + a_1 X_{t-1} + \beta_1 Precip_{t-1}$	0.57	117.41	-1.48 [-2.17, -0.81]	-0.57 [-1.10, -0.03]	-	0.27 [-0.24, 0.77]
$X_t \sim a_0 + a_1 X_{t-1} + a_2 X_{t-2}$	**0.00***	**116.85***	-1.68 [-2.87, -0.55]	-0.57 [-1.23, 0.08]	-0.26 [-0.90, 0.38]	-
$X_t \sim a_0 + a_1 X_{t-1}$	0.11	116.96	-1.46 [-2.17, -0.78]	-0.53 [-1.06, -0.03]	-	-
$X_t \sim a_0 + \beta_1 Precip_{t-1}$	0.72	117.57	-0.17 [-1.06, 0.72]	-	-	0.09 [-0.81, 0.98]
$X_t \sim a_0$	0.81	117.66	-0.18 [-1.03, 0.68]	-	-	-
2004-2019:						
$X_t \sim a_0 + a_1 X_{t-1} + a_2 X_{t-2} + \beta_1 Precip_{t-1}$	**0.00***	**86.32***	-0.58 [-1.98, 0.79]	0.46 [-0.05, 0.96]	-0.19 [-0.74, 0.36]	0.92 [0.01, 1.87]
$X_t \sim a_0 + a_1 X_{t-1} + \beta_1 Precip_{t-1}$	1.65	87.97	-0.22 [-1.50, 0.96]	0.60 [0.01, 1.15]	-	1.14 [0.24, 1.15]
$X_t \sim a_0 + a_1 X_{t-1} + a_2 X_{t-2}$	0.53	86.85	-1.30 [-2.78, 0.06]	0.340 [-0.23, 0.89]	-0.46 [-1.02, 0.01]	-
$X_t \sim a_0 + a_1 X_{t-1}$	1.13	87.45	-0.72 [-2.27, 0.71]	0.35 [-0.32, 1.00]	-	-
$X_t \sim a_0 + \beta_1 Precip_{t-1}$	1.76	88.08	0.45 [-0.35, 1.23]	-	-	1.37 [0.45, 2.28]
$X_t \sim a_0$	1.02	87.34	0.33 [-0.79, 1.46]	-	-	-

Table S1. Results of Bayesian state space time series model selection, by period of series analyzed and the process model structure. Change in WAIC relative to the best model (ΔWAIC), WAIC, and parameter estimates with 95% posterior intervals are shown. WAIC values within ΔWAIC <2 of the best model are bolded, and the best model is bolded. Parameter estimates the 95% posterior intervals which do not overlap zero are bolded as well.

Series	Original	Whole series, fitted β_1	Part I, fitted β_1	Part II, fitted β_1	Whole series, equal β_1	Part I, equal β_1	Part II, equal β_1	Part II, no a_1, a_2
Original	0							
Whole series, fitted β_1	22.14	0						
Part I, fitted β_1	22.80	10.38	0					
Part II, fitted β_1	**17.55**	10.17	16.51	0				
Whole series, equal β_1	18.54	11.87	15.89	11.30	0			
Part I, equal β_1	21.42	19.56	18.19	16.44	17.58	0		
Part II, equal β_1	**17.55**	10.17	16.51	0	6.22	16.5	0	
Part II, no a_1, a_2	19.72	12.73	15.84	6.52	6.37	13.75	6.67	0

Table S2. Dissimilarity matrix of simulated time series from fitted state-space process models, with original fitted parameters and with effect of precipitation set to equal at the highest fitted value (β_1=0.922), all compared with the original observed time series. Lowest dissimilarities relative to the original series for simulations with fitted or equal β_1 values are bolded.

Series	*Parameter*	a_0	a_1	a_2	β_1
Whole Series	a_0	1			
	a_1	0.584	1		
	a_2	0.551	-0.014	1	
	β_1	0.109	0.001	0.157	1
Part I	a_0	1			
	a_1	0.744	1		
	a_2	0.739	0.465	1	
	β_1	-0.116	-0.214	-0.049	1
Part II	a_0	1			
	a_1	0.491	1		
	a_2	0.628	-0.116	1	
	β_1	0.501	0.207	0.520	1

Table S3. Cross-correlation matrices between parameter estimates from MCMC chains the full state space model from the whole series, part I and part II.

526

Year	Caterpillar count	Lupine area (m^2)
1986	490	400
1987	8	101.35
1988	12	53.75
1989	25	51
1990	48	61.24
1991	7	41.5
1992	71	63.75
1993	5	29.25
1994	16	59.75
1995	15	20.5
1996	40	18.05
1997	2	20
1998	8	20
1999	12	18
2000	8	38
2001	40	31.5
2002	18	63
2003	52	45.5
2004	3	64.5
2005	0	57.5
2006	2	34
2007	51	35
2008	40	32.5
2009	9	62
2010	2	51.5
2011	23	27.75
2012	27	15.5
2013	2	40
2014	8	33
2015	3	29.5
2016	13	38
2017	7	30
2018	22	21
2019	131	26

527 **Table S4**. Year, caterpillar counts, and area of lupine surveyed.

528

529

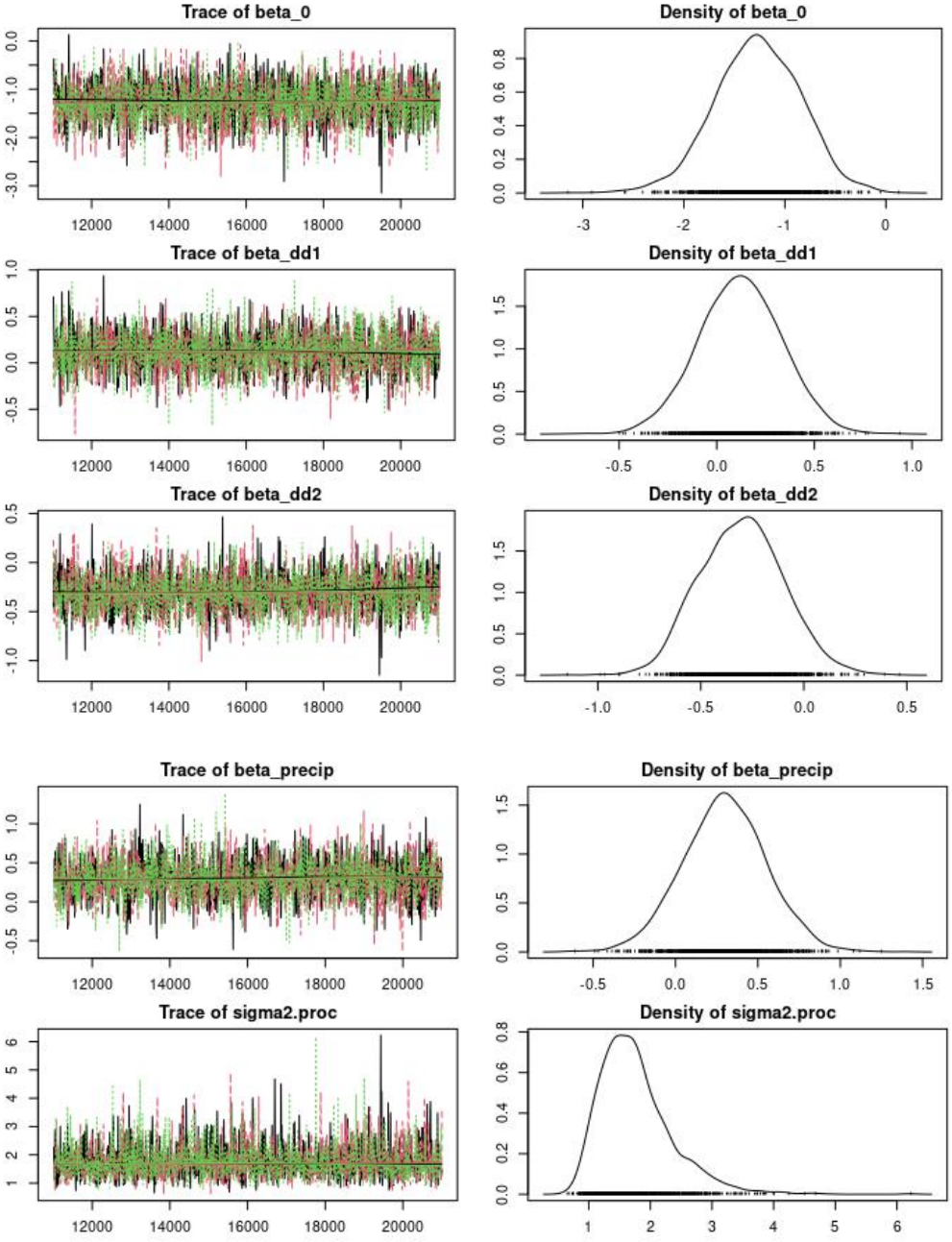

Figure S1. MCMC trace and density plot of parameters from full state space model of the whole series.

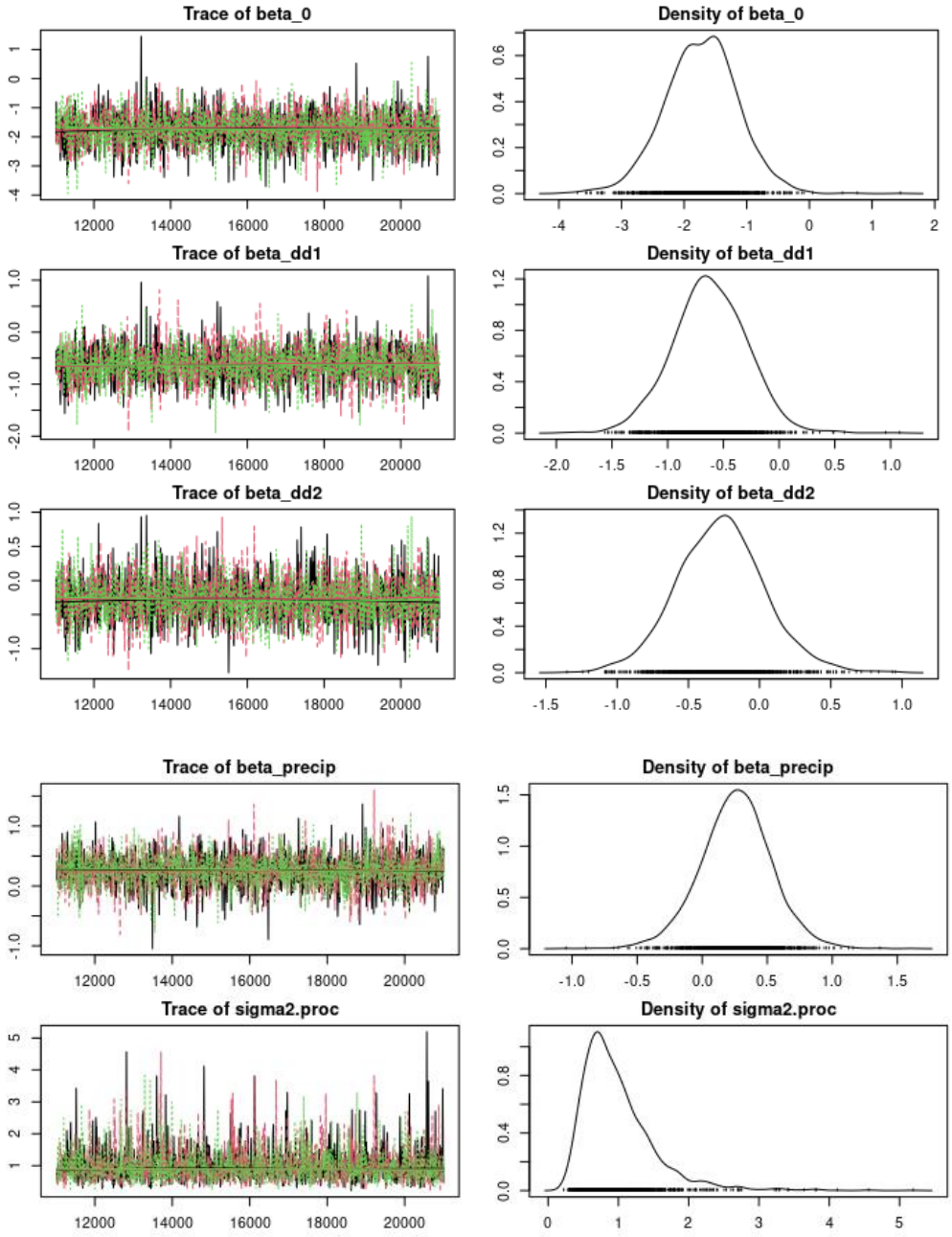

Figure S2. MCMC trace and density plots of parameters from full state space model of the first part of the series.

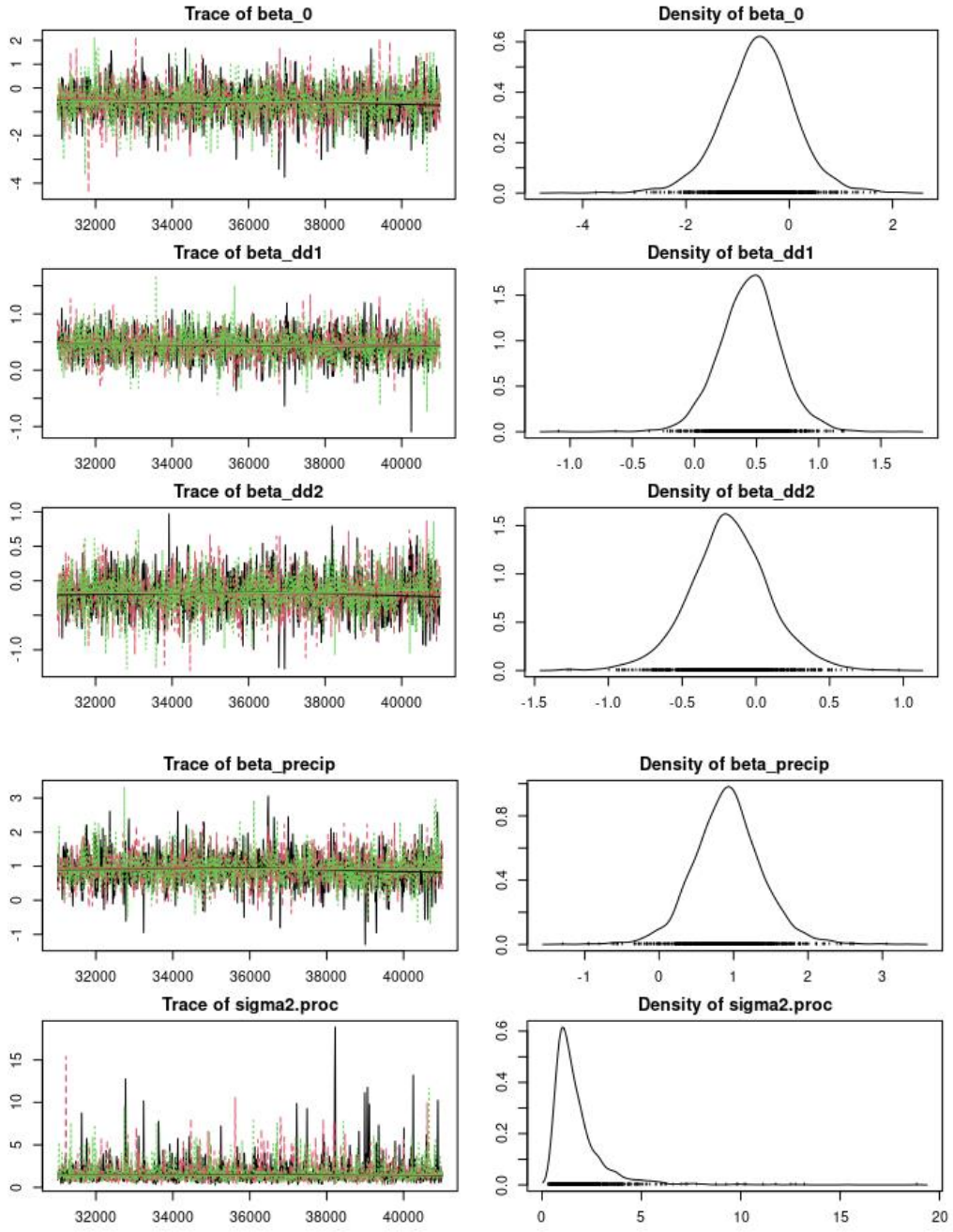

Figure S3. MCMC trace and density plots of parameters from full state space model of the second part of the series.

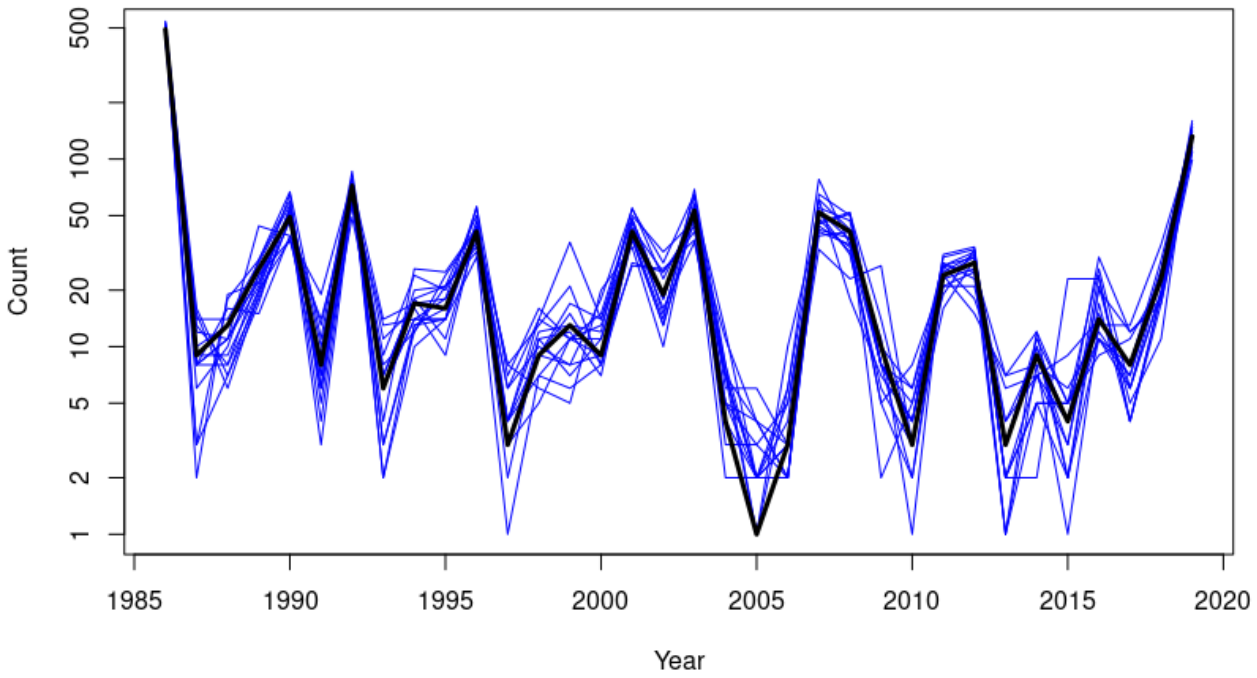

Figure S4. Posterior predictive simulations from full state space model of the whole series, with the observed trajectory in black, and one-step ahead simulations from 15 draws from the posterior in blue.

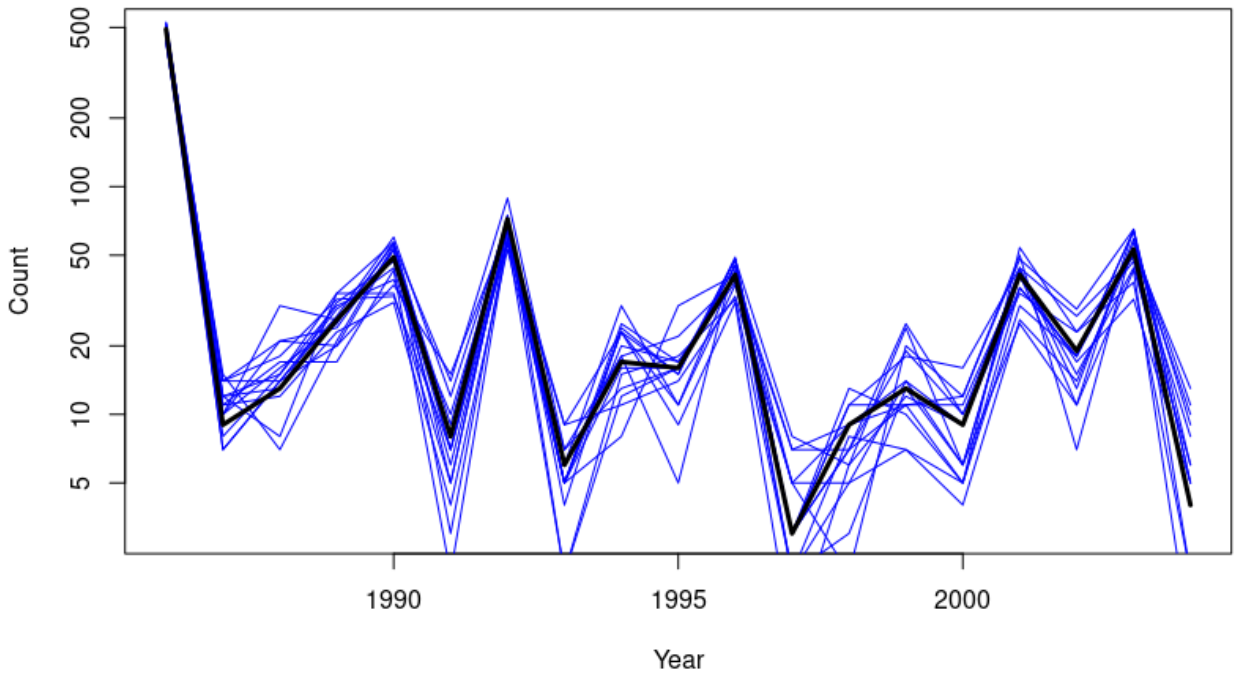

549

550 **Figure S5.** Posterior predictive simulations from full state space model of the first part of the series,

551 with the observed trajectory in black, and one-step ahead simulations from 15 draws from the posterior

552 in blue.

553

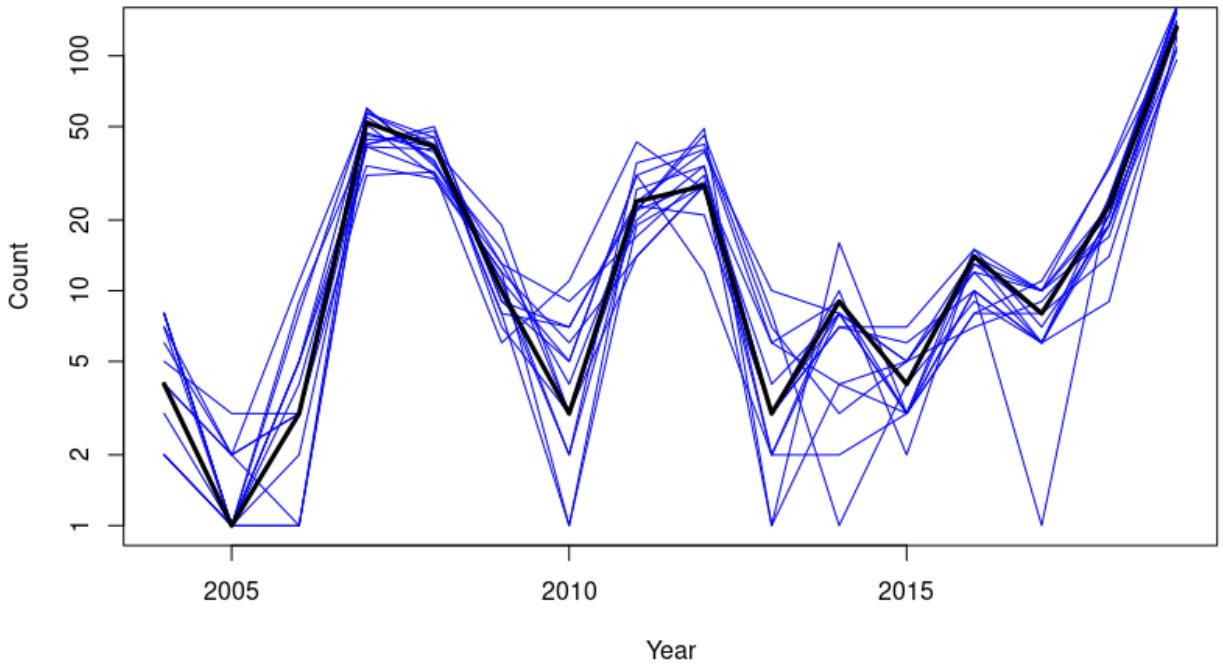

554

555 **Figure S6**. Posterior predictive simulations from full state space model of the second part of the series,

556 with the observed trajectory in black, and one-step ahead simulations from 15 draws from the posterior

557 in blue.

558

559

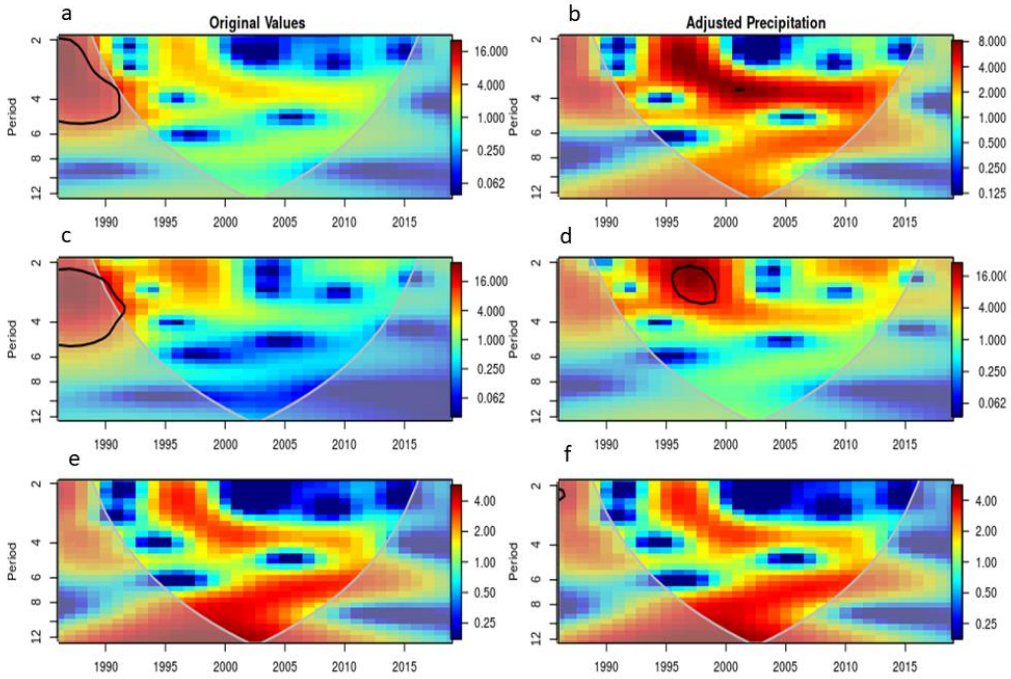

Figure S7. Wavelet transformations of simulated trajectories from fitted state-space process models. (a,c,e) Simulations using original fitted values, and (b,d,f) using fitted values for density-dependence but the highest values for precipation. (a,b) Models of the whole series, (c,d) before the threshold, and (e,f) after the threshold. Black lines delimit regions of significant periodicity or coherence at a 95% confidence level from a bootstrap test. Color bars show the scale for power from low (blue) to high (red).

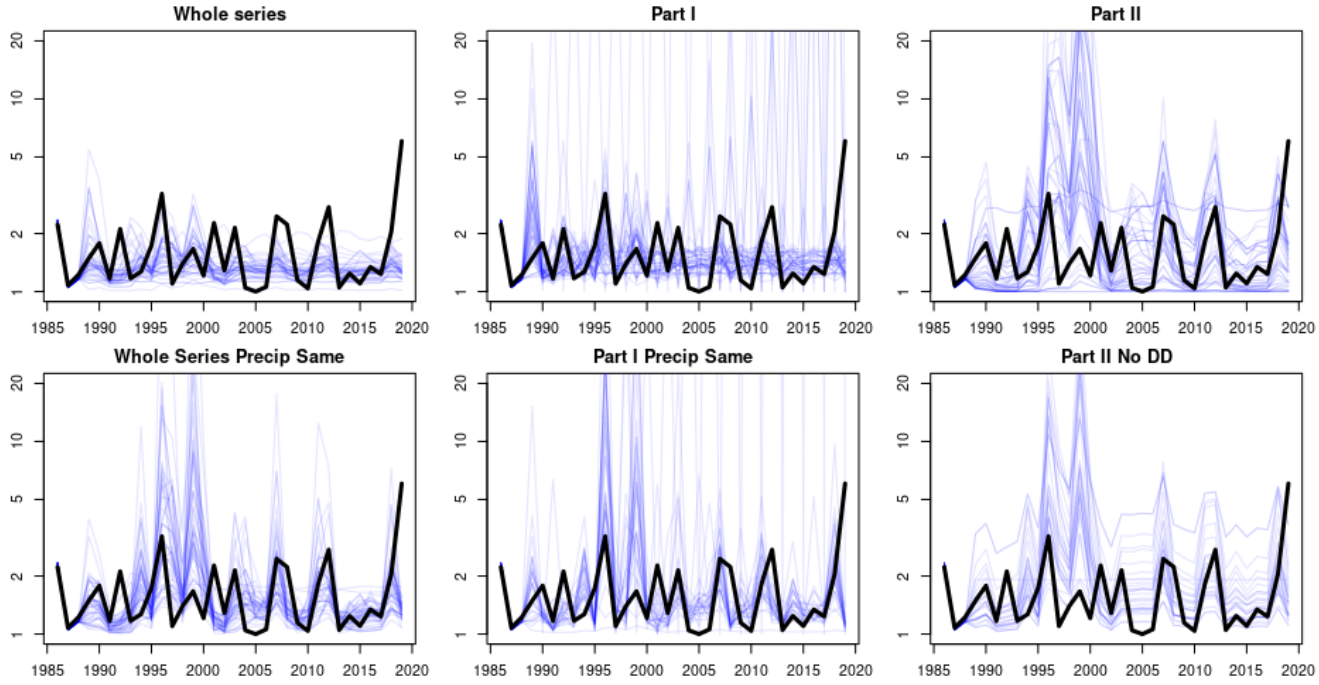

568

569 **Figure S8.** Fifty simulation trajectory results (blue) vs. true population trajectory (black) from

570 simulation based on the models (left to right, top to bottom) from the whole series, part I, part II , the

571 whole series with precipitation values from part II, part I with precipitation values from part II, and part

572 II without density dependence.

573